Supporting Information

Highly stable Graphene Oxide Composite Nanofiltration Membrane

KaiQiang Zheng[a], ShiQing Li[a], Zhou Chen[a,*], YunQiang Chen[b], YuBin Hong[b,*], WeiGuang Lan[a, b,*]

[a] Mr. K.Q. Zheng, Mr. S.Q. Li, Dr. Z. Chen, Prof. W.G. Lan
Xiamen University Center for Membrane Application and Advancement, College of Materials, Xiamen University, Xiamen 361005, Fujian, China.
[b] Mr. Y.Q. Chen, Mr. Y.B. Hong
Suntar Membrane Technology (Xiamen) Co., Ltd., Xiamen 361022, Fujian, China.
Corresponding authors: Dr. Z. Chen (zhouchen@xmu.edu.cn); Mr. Y.B. Hong (hongyb@suntar.com); Prof. W.G. Lan (wglan@xmu.edu.cn).

1. Experimental part

1.1 Membrane fabrication

Preparation of GO. GO was prepared by modified Hummers method[1]. Typically, 6 g flake graphite, 720 mL H_2SO_4 (98%) and 80 mL H_3PO_4 were added into 2000 mL beaker, then 36 g $KMnO_4$ was slowly added into the mixture with mechanically stir. After mixing evenly, the beaker was put in oil bath and stirred at 50 °C for 12 h, and then cooled the solution to room temperature. Diluted 8 mL 30%H_2O_2 into 800 mL and froze it into ice block. Slowly mixed the GO solution into the H_2O_2 ice block, then added the same concentration of H_2O_2 solution into the beaker and kept stirring until the solution turned bright yellow. The solution was washed by cross flow in 50 nm ceramic filter tube to remove the impurity. Finally, the obtained GO solution was centrifuged and concentrated to prepare the standard solution. The average size of GO nanosheet was 2-5 μm (Figure S1).

Preparation of G-TX solution. G-TX was prepared by in-situ hydrothermal growth of TiO_2 nanocrystals on GO nanosheet[2]. Typically, a certain ratio of $Ti(SO_4)_2$ and GO were mixed under ice water bath. After 30 min ultrasonic treatment, the mixture was transferred to 60 ℃ oil bath and stirred 24 h. The solution was washed and centrifugated to move the impurities to obtain G-TX, where X (X=2, 3, 4 and 5) represents the mass ratio of $Ti(SO_4)_2$ to GO. Subsequently, the solid content of G-TX solution was diluted to 1 mg/mL. The schematic diagrams of GO and G-TX are shown in Figure S2 (a-e).

Preparation of G-TX based membrane. A vacuum filtration method was used to fabricate the G-TX based membrane, the effective area of membrane is controlled as

13.08 cm^2. Take G-T3 membrane as an example, 2 mL G-T3 solution (1 mg/mL) was diluted to 20 mL, then ultrasonic dispersion was performed for 5 mins to get uniform G-T3 suspension. To form G-T3 membrane, the suspension was slowly poured onto the supporting CA membrane, and turned on the vacuum filter and completed the filtration after the suspension in the suction cup was drained. The preparation of the other G-TX membrane is similar to the G-T3 membrane, except for the G-TX solution used.

Preparation of G-TX-PY membrane. Detailly, 1 mL of 1 mg/mL PEI solution was diluted to 10 mL, and poured it slowly on the surface of G-TX membrane along the wall of suction cup. After standing for 5 minutes, turned on the filter switch to pump the water and grafted the PEI on the surface of the G-TX-PY membrane, where Y=1, 2, 3, 4 represent the 600, 1800, 10000, 70000 MW of PEI, respectively (Diagrams shown in Figure S 2f). The obtained membrane was washed three times by reverse osmosis water to remove the excess unreacted PEI.

1.2 Characterization

The SEM morphology of samples were carried on Hitachi SU-70. Transmission electron microscopy (TEM) was carried on Hitachi H9500. Thermogravimetric analysis (TGA) was performed on STA449F3. X-ray diffraction (XRD) was carried on Bruker-axes (Cu Kα radiation, 40 kV, 40 mA). Fourier transform infrared spectroscopy (FT-IR) was analyzed by IS10. The X-ray photoelectron spectroscopy (XPS) was performed on PHI Quantum 2000 Scanning ESCA Microprobe. Al-Kα radiation was used as the X-ray source and the binding energies were referenced to the C 1s peak (284.6 eV). The surface roughness of the membrane was measured by atomic force microscope (AFM,

Keysight MI5500). The contact angle (CA) was measured on DSA100 instrument. The N_2 adsorption and desorption experiments was measured on Best Instrument 3H-2000PM2.

1.3 Membrane flux and separation performance test

The dead-end filtration method[3] was used to measure the pure water flux and dye retention, the pure water flux is calculated by the following formula:

$$J = \frac{v}{A \times t \times P}$$

Where J, V, A, t, P represent the pure water permeance (L m^{-2} h^{-1} bar^{-1}), liquid volume (L) through the membrane, effective area of the membrane (13.08 cm^2), time (0.5 h) and operating pressure (1 bar), respectively.

Dye retention rate was determined by filtering 10 mg L^{-1} target dye through the membrane. The rejection rate was calculated by the following formula:

$$R = \left(1 - \frac{Cp}{Cf}\right) \times 100\%$$

Where C_P and C_f represent the dye concentration of the permeate side and the feed side, respectively.

1.4 Membrane reusability test

The reusability of G-TX-PY membrane was investigated by filtration-dry-filtration process. After the first filtration, the feed liquid was poured out and the adsorbed water between layers was pumped out, then the membrane was stood 30 mins at room temperature to complete one cycle. Importantly, for the using scene of industrial membrane component, it is a necessary to take the membrane core out of the membrane pool during cleaning, meaning that a membrane that can keep in dry condition would

meet the real operational process. Therefore, the stability test process proposed here meets practical value for the industrial application of GO membrane.

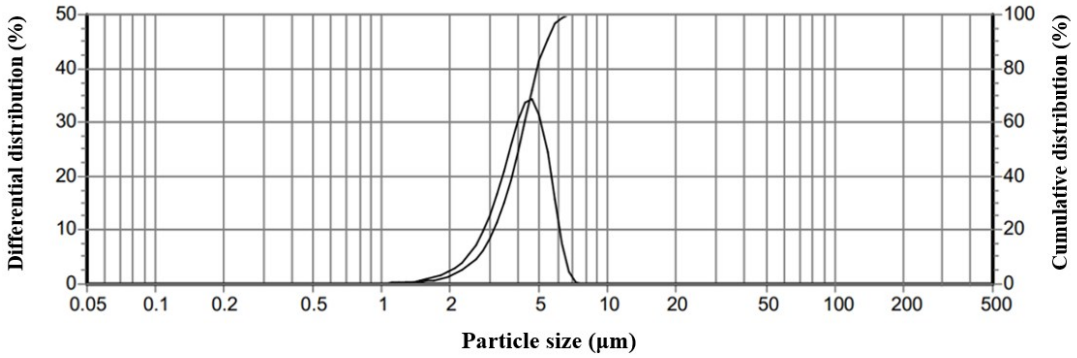

Figure S1. Laser particle size distribution of GO. The nanosheet size of GO is distributed in 2-5 μm.

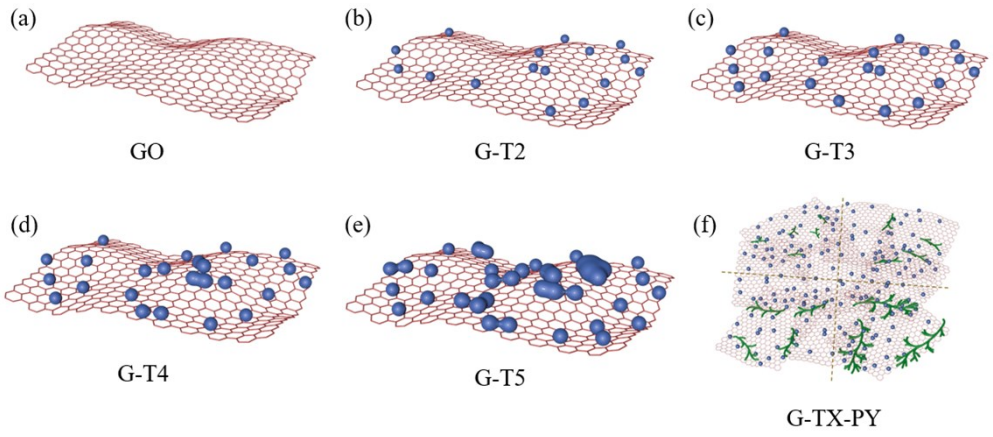

Figure S2. Graphical diagrams of (a) GO, (b) G-T2, (c) G-T3, (d) G-T4, (e) G-T5 and (f) G-TX-PY.

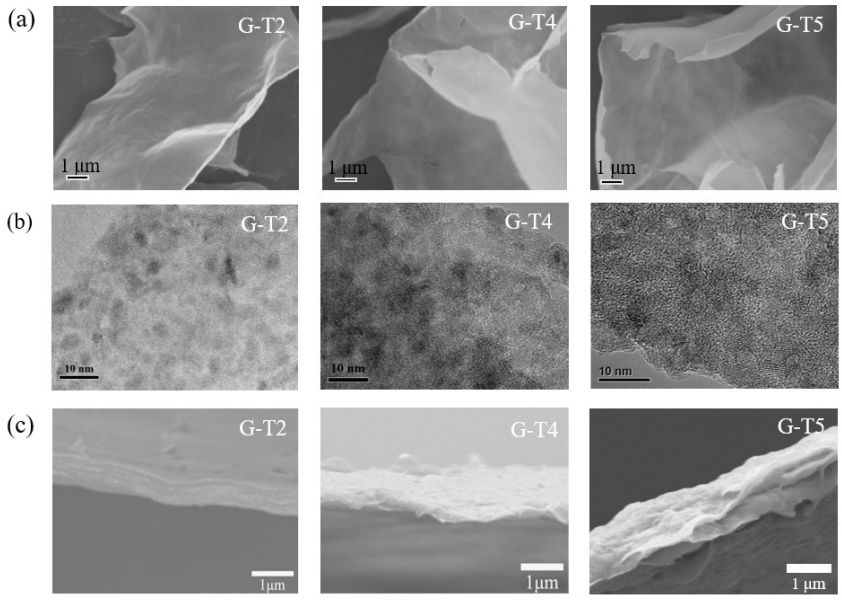

Figure S3. Surface and cross section morphology of the composite membranes. (a) SEM, (b) TEM and (c) cross-sectional SEM images of G-T2, G-T4 and G-T5.

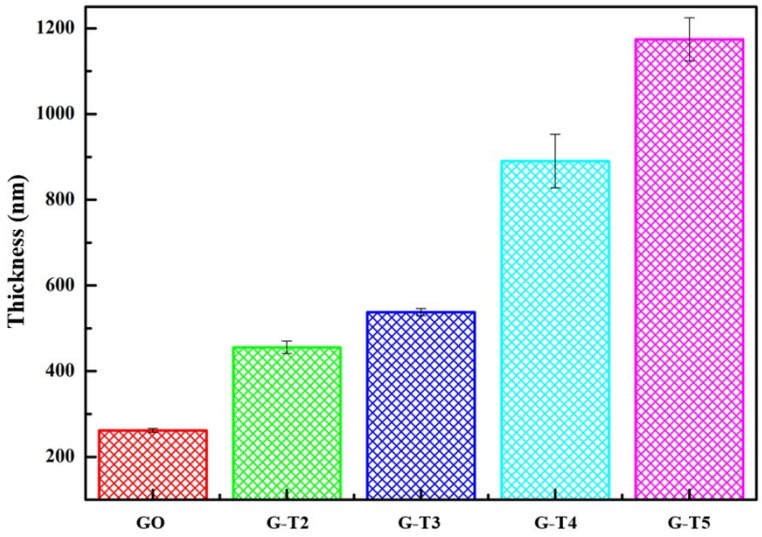

Figure S4. The thickness of G-TX based membranes. The thickness of G-TX membranes was quantitatively measured by taking the average value of five positions on the cross-section images.

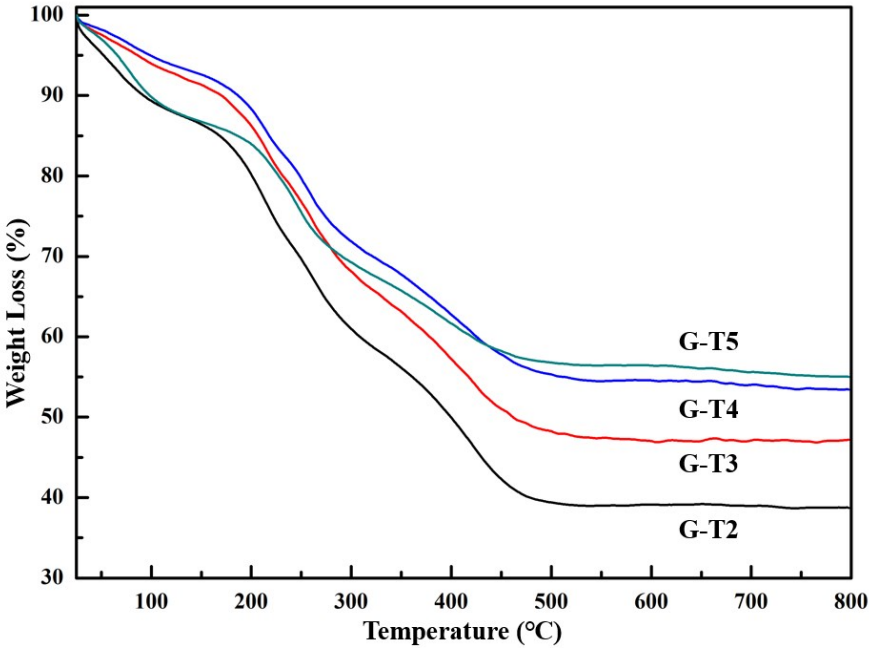

Figure S5. TG curves of G-TX.

We qualitatively analyzed the weight percentage of different G-TX membrane by TGA (Figure S5). The weight loss process of G-TX can be divided into two stages, that is, the removal of surface adsorbed water from 26 ℃ to 120 ℃ and the decomposition of GO from 120 ℃ to 460 ℃ [2]. As the TiO_2 can stable existence below 700 ℃ [4], we can quantify the weight percentage of various G-TX composite membranes. As results, the weight content of TiO_2 increased from 38.7% for G-T2 to 55.1% for G-T5. These results are highly consistent with the thickness study.

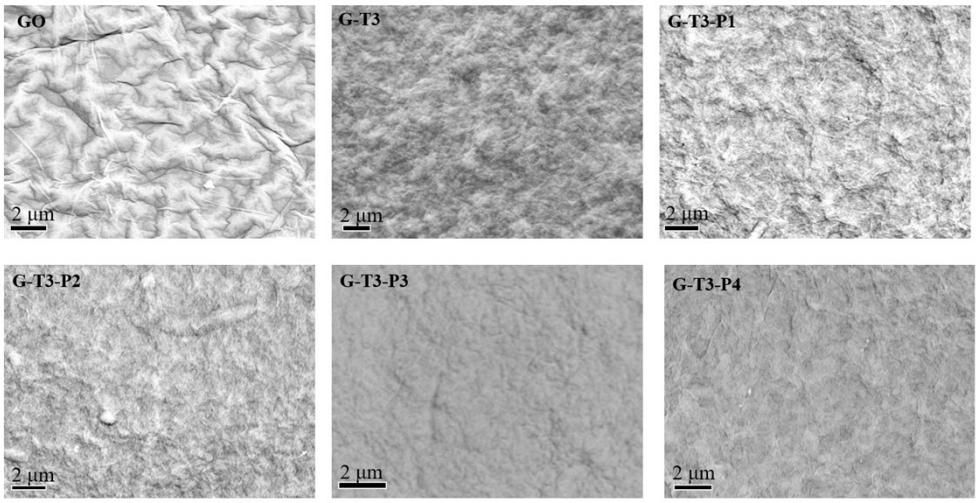

Figure S6. SEM images of GO, G-T3 and G-T3-PY based membranes.

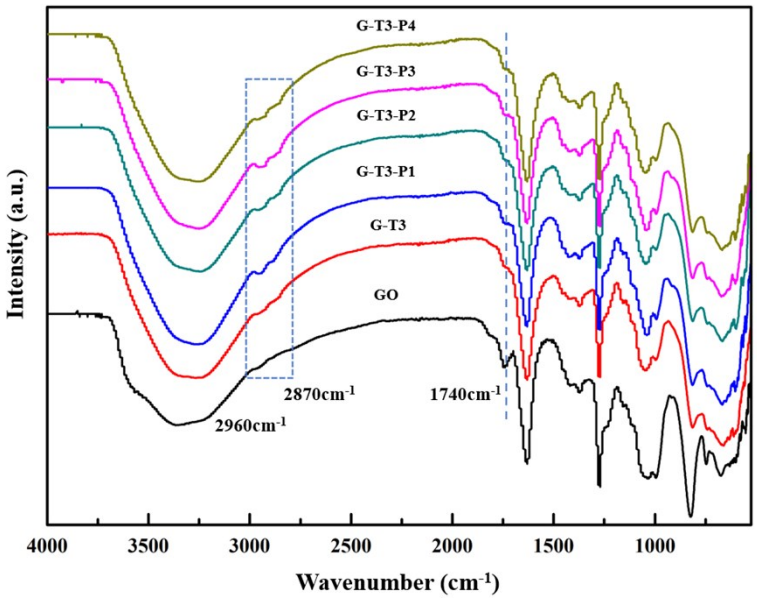

Figure S7. FT-IR patterns of GO, G-T3 and G-T3-PY based membranes.

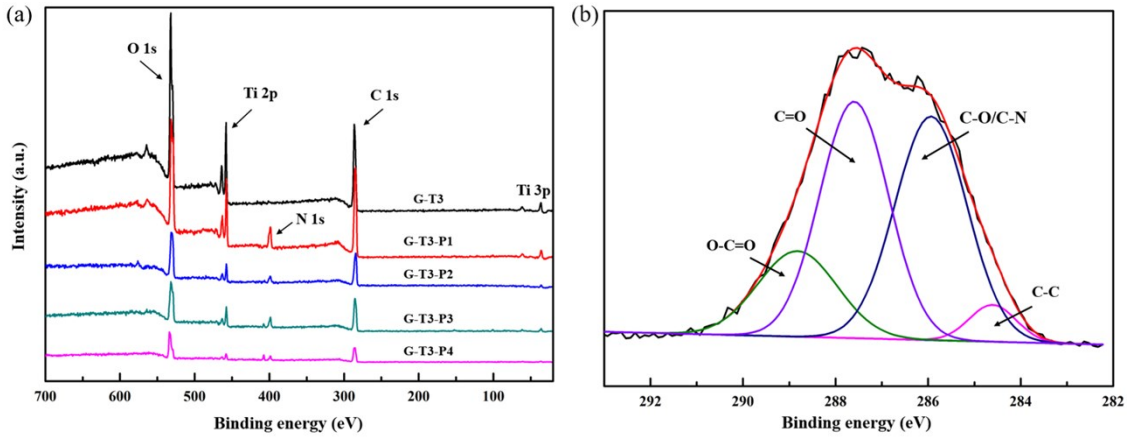

Figure S8. (a) XPS full spectrum of G-T3 and G-T3-PY membranes. (b) The de-convolution of C 1s of G-T3-P4 membrane.

The peak at 1740 cm^{-1} in FT-IR is the C=O vibration of the GO structure (Figure S7). The C=O vibrational peak intensity decreased for the G-T3-PY membranes, indicating that the GO lamellae may partial reduce during hydrothermal formation of TiO_2 according to previous literature[5]. In addition, two peaks at 2960 cm^{-1} and 2870 cm^{-1} can be ascribed to the CH_2 vibration [6], indicating that PEI is successfully bonded onto the surface of the membrane, which is highly related to the XPS discussions (Figure S8-10).

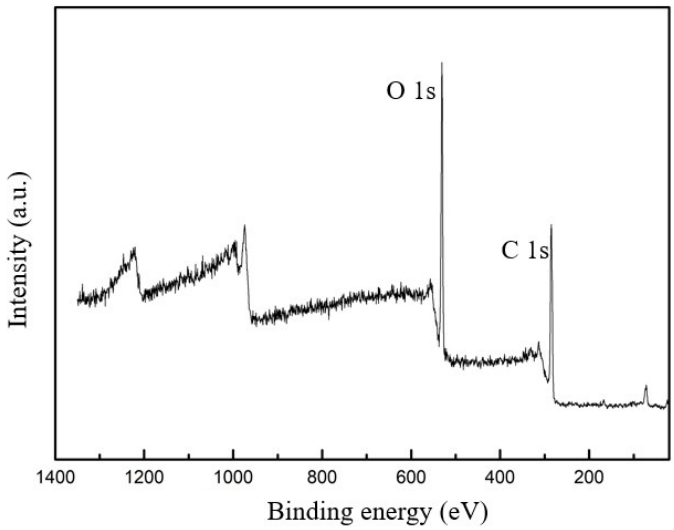

Figure S9. Full XPS spectrum of GO.

The surface elements of G-T3-PY composite nanofiltration membrane were further analyzed by XPS. As is shown in Figure S8a. The signals of Ti 2p, O 1s, N 1s and C 1s can be observed in the XPS full spectrum[7-9]. The existence of Ti element further confirms the successful growth of the TiO_2 nanocrystals onto GO lamellae. Comparison of the full XPS spectrum of G-T3-PY, G-T3 and GO (Figure S9), the appearing of N 1s signal in G-T3-PY indicates that PEI was successfully encapsulated on the surface of the composite membrane. The C 1s of G-T3-P4 is shown in Figure S8b. The corresponding C 1s curve has 4 peaks located at 284.6, 285.9, 287.6 and 288.8 eV, which are ascribed to C-C, C-O/C-N, C=O and O-C=O, respectively[10]. The fitting results indicate that inserting TiO_2 nanocrystals to the GO interlayers does not destroy the functional groups of GO. Besides, the existence of C-N bond also illustrates the successful loading of PEI on G-T3-P4 composite membrane.

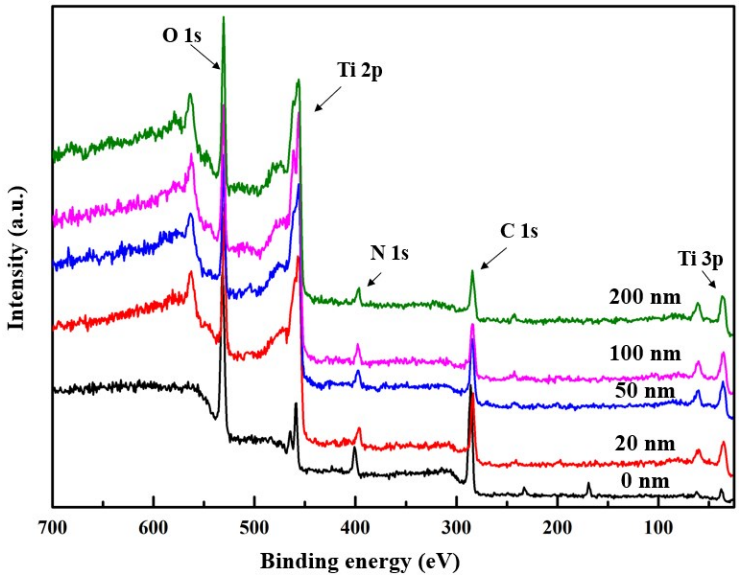

Figure S10. XPS spectra of G-T3-P4 at 0, 20, 50, 100 and 200 nm sputtering depths.

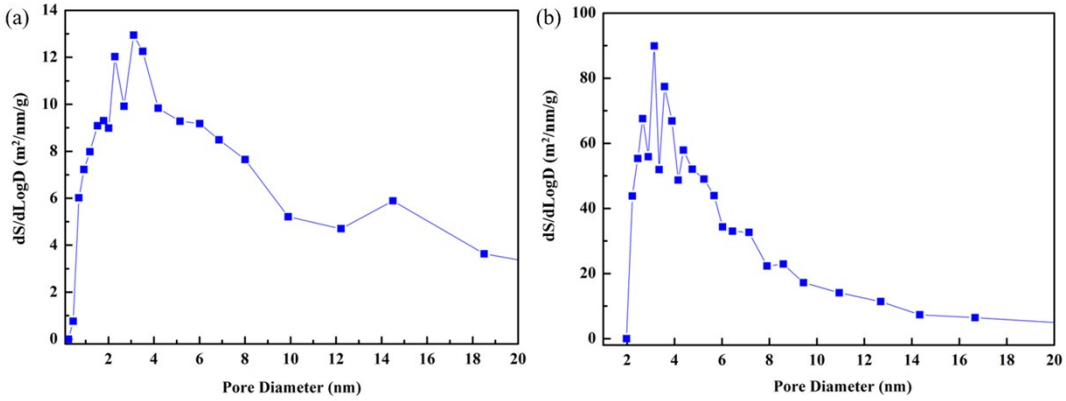

Figure S11. Pore size distribution of (a) GO membrane (b) G-T3-P4 composite nanofiltration membrane.

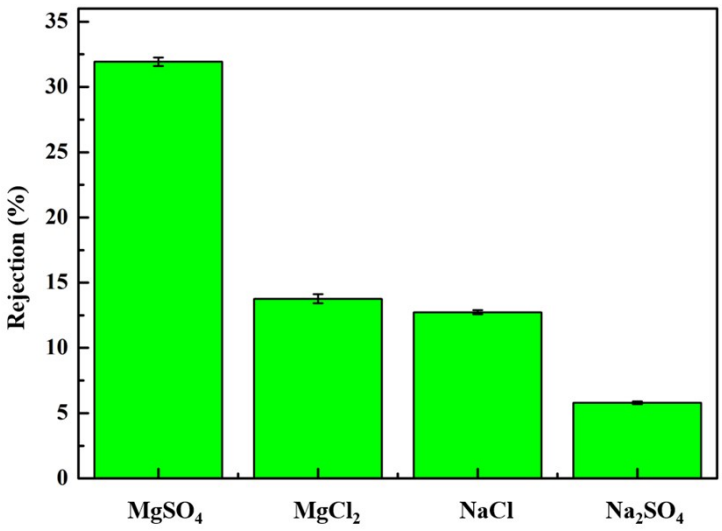

Figure S12. Rejection of 2000 ppm salt solution by G-T3-P4 composite nanofiltration membrane

Table S1. Separation performance of the state-of-the-art GO based membranes.

Membranes	Operational condition	Flux (L m^{-2} h^{-1} bar^{-1})	Rejection rate (%)	Refs
GO/MoS_2	2 bar	10.2±1.68	10 mg/L CR (99.6) MB (97.4) Na_2SO_4 (65.2) NaCl (43.2)	11
PAA/GO	4.9 bar	27.7 23.5	200 ppm Na_2SO_4 (99) 2000 ppm Na_2SO_4 (79)	12
CNC/TFC/Ms	2 bar	16	10 ppm MO (100) 2 g L^{-1} Na_2SO_4 (67)	13
GO/PI	15 bar	7.70	200 ppm orange II sodium (56.6) Safranin O (86.52) Solvent blue 35 (4.39) Rhodamine B (66.95) Remazol brilliant blue (97.11)	14
OAGO/EDA	Pervaporation	1.12	(Na^+, K^+, Mg^{2+}, Cl^-, $SO4^{2-}$) ion (>98.1)	15
GO/PNIPAM	1 bar	12.4 (25 ℃)	25 ℃ 4 mg L^{-1} RB (68.2) 40 mg L^{-1} CBB (98.0)	16

		1.81 (50 ℃)	100 mg L^{-1} Cyt (99.8) 50 ℃ 4 mg L^{-1} RB (100) 40 mg L^{-1} CBB (100) 100 mg L^{-1} Cyt (100)	
CDA-GO	Pervaporation	20	3.5 wt% sea water (99.9)	[17]
TiO_2@GO	4 bar	22.43	1 g/L Na_2SO_4 (99.8)	[8]
GO@PAN	1 bar	11.13	10 mg/L NaCl (27.86) Evans blue (99.99)	[18]
GO/Surfactant	5 bar	20.0	$MgCl_2$ (32)	[19]
G-T3-P4	1 bar	26.0	10 mg/L MB (99.9) 10 mg/L Eosin (99.9)	This work

References

1. D. C. Marcano, D. V. Kosynkin, J. M. Berlin, A. Sinitskii, Z. Sun, A. Slesarev, L. B. Alemany, W. Lu and J. M. Tour, ACS Nano, 2010, 4, 4806-4814.
2. C. Xu, A. Cui, Y. Xu and X. Fu, Carbon, 2013, 62, 465-471.
3. Y. Han, Z. Xu and C. Gao, Adv. Funct. Mater., 2013, 23, 3693-3700.
4. J. R. McCormick, B. Zhao, S. A. Rykov, H. Wang and J. G. Chen, J. Phys. Chem. B., 2004, 108, 17398-17402.
5. Z. Lin, Y. Yao, Z. Li, Y. Liu, Z. Li and C.-P. Wong, J. Phys. Chem. C., 2010, 114, 14819-14825.
6. L. Xue, N. P. Ingle and T. M. Reineke, Biomacromolecules, 2013, 14, 3903-3915.

7. Y. Liu, X. Cai, B. Luo, M. Yan, J. Jiang and W. Shi, Carbon, 2016, 107, 426-432.

8. J. Wang, Y. Wang, J. Zhu, Y. Zhang, J. Liu and B. Van der Bruggen, J. Membr. Sci., 2017, 533, 279-288.

9. H. Niu, Y. Zhang, Y. Liu, B. Luo, N. Xin and W. Shi, J. Mater. Chem. A., 2019, 7, 8503-8509.

10. R. Zhang, Y. Li, Y. Su, X. Zhao, Y. Liu, X. Fan, T. Ma and Z. Jiang, J. Mater. Chem. A., 2016, 4, 7892-7902.

11. P. Zhang, J.-L. Gong, G.-M. Zeng, B. Song, W. Cao, H.-Y. Liu, S.-Y. Huan and P. Peng, J. Membr. Sci., 2019, 574, 112-123.

12. F. Baskoro, C.-B. Wong, S. R. Kumar, C.-W. Chang, C.-H. Chen, D. W. Chen and S. J. Lue, J. Membr. Sci., 2018, 554, 253-263.

13. Q. Zhang, S. Chen, X. F. Fan, H. G. Zhang, H. T. Yu and X. Quan, Appl. Catal. B-Environ., 2018, 224, 204-213.

14. B. Li, Y. Cui, S. Japip, Z. Thong and T.-S. Chung, Carbon, 2018, 130, 503-514.

15. H. Lin, S. Dangwal, R. Liu, S.-J. Kim, Y. Li and J. Zhu, J. Membr. Sci., 2018, 563, 336-344.

16. J. Liu, N. Wang, L. J. Yu, A. Karton, W. Li, W. Zhang, F. Guo, L. Hou, Q. Cheng, L. Jiang, D. A. Weitz and Y. Zhao, Nat Commun, 2017, 8, 2011.

17. Y. Qian, C. Zhou and A. Huang, Carbon, 2018, 136, 28-37.

18. J. Q. Wang, P. Zhang, B. Liang, Y. X. Liu, T. Xu, L. F. Wang, B. Cao and K. Pan, ACS. Appl. Mater. Inter., 2016, 8, 6211-6218.

19. B. Lian, J. Deng, G. Leslie, H. Bustamante, V. Sahajwalla, Y. Nishina and R. K. Joshi, Carbon, 2017, 116, 240-245.